Article (refereed) - postprint

Title

1

The persistence of carbon in the African forest understory

3

Authors

5 Wannes Hubau [1,2,3] *, Tom De Mil [1,2] *, Jan Van den Bulcke [2,4], Oliver L. Phillips [3], Bhély Angoboy Ilondea

6 [1,5,6], Joris Van Acker [2,4], Martin J. P. Sullivan [3], Laurent Nsenga [1], Benjamin Toirambe [1], Camille Couralet [1],

7 Lindsay F. Banin [7], Serge K. Begne [8,3], Timothy R. Baker [3], Nils Bourland [1,9,10,11], Eric Chezeaux [12], Connie

8 J. Clark [13], Murray Collins [14], James A. Comiskey [15,16], Aida Cuni-Sanchez [17,18], Victor Deklerck [2,4], Sofie

9 Dierickx [1], Jean-Louis Doucet [10], Corneille E. N. Ewango [19,20,21], Ted R. Feldpausch [22], Martin Gilpin [3],

10 Christelle Gonmadje [23], Jefferson S. Hall [24], David J. Harris [25], Olivier J. Hardy [26], Marie-Noel D. Kamdem

11 [8,27], Emmanuel Kasongo Yakusu [1,21,2], Gabriela Lopez-Gonzalez [3], Jean-Remy Makana [19], Yadvinder Malhi

12 [28], Faustin M. Mbayu [21], Sam Moore [28], Jacques Mukinzi [19,29], Georgia Pickavance [3], John R. Poulsen [13], Jan

13 Reitsma [30], Mélissa Rousseau [1,11], Bonaventure Sonké [8], Terry Sunderland [9,31], Hermann Taedoumg [8], Joey

14 Talbot [3], John Tshibamba Mukendi [1,21,32], Peter M. Umunay [33], Jason Vleminckx [26,34], Lee J. T. White [35,36,37],

15 Lise Zemagho [8], Simon L. Lewis [3,17], Hans Beeckman [1]

16

17 * These authors contributed equally to this work.

18

Contact information

20 whubau@gmail.com, wannes.hubau@africamuseum.be, tom.demil@ugent.be

21 Service of Wood Biology, Royal Museum for Central Africa

22 Tervuren, Belgium, Leuvensesteenweg 13, 3080 Tervuren

23

Affiliations

25 1 Service of Wood Biology, Royal Museum for Central Africa, Tervuren, Belgium

26 2 UGent-Woodlab, Laboratory of Wood Technology, Department of Environment, Ghent University,

27 Ghent, Belgium

28	3	School of Geography, University of Leeds, Leeds, UK
29	4	Centre for X-ray Tomography (UGCT), Ghent University, Ghent, Belgium
30	5	Institut National pour l'Etude et la Recherche Agronomique, Kinshasa I, Democratic Republic of
31		Congo
32	6	Ecole Régionale Postuniversitaire d'Aménagement et de Gestion intégrés des Forêts et Territoires
33		tropicaux (ERAIFT), Kinshasa, Democratic Republic of Congo
34	7	Centre for Ecology and Hydrology, Penicuik, UK
35	8	Plant Systematic and Ecology Laboratory, Higher Teachers' Training College, University of
36		Yaounde I, Cameroon
37	9	CIFOR, Bogor, Indonesia
38	10	Forest Resources Management, Gembloux Agro-Bio Tech, University of Liege, Belgium
39	11	Resources and Synergies Development, Singapore, Singapore
40	12	Rougier-Gabon, Libreville, Gabon
41	13	Nicholas School of the Environment, Duke University, Durham, NC, USA
42	14	Grantham Research Institute on Climate Change and the Environment, London, UK
43	15	Inventory & Monitoring Program, National Park Service, Fredericksburg, VA, USA
44	16	Smithsonian Institution, Washington, DC, USA
45	17	Department of Geography, University College London, London, UK
46	18	Department of Geography and Environment, University of York, York, UK
47	19	Wildlife Conservation Society-DR Congo, Kinshasa I, Democratic Republic of Congo
48	20	Centre de Formation et de Recherche en Conservation Forestiere (CEFRECOF), Epulu, Democratic
49		Republic of Congo
50	21	Faculté de Gestion de Ressources Naturelles Renouvelables, Université de Kisangani, Kisangani,
51		Democratic Republic of Congo
52	22	Geography, College of Life and Environmental Sciences, University of Exeter, Exeter, UK
53	23	National Herbarium, Yaounde, Cameroon
54	24	ForestGEO, Smithsonian Tropical Research Institute, Panamá, Republic of Panama
55	25	Royal Botanic Garden Edinburgh, Edinburgh, UK

56 26 Service d'Évolution Biologique et écologie, Faculté des Sciences, Université Libre de Bruxelles,

57 Brussels, Belgium

58 27 Faculty of Science, Department of Botany and Plant Physiology, University of Buea, Buea,

59 Cameroon

60 28 Environmental Change Institute, School of Geography and the Environment, University of Oxford,

61 Oxford, UK

62 29 Salonga National Park, Kinshasa I, DR Congo

63 30 Bureau Waardenburg, The Netherlands

64 31 Faculty of Forestry, University of British Columbia, Vancouver, Canada

65 32 Faculté des Sciences Appliquées, Université de Mbujimayi, Mbujimayi, Democratic Republic of

66 Congo

67 33 Yale School of Forestry & Environmental Studies, New Haven, CT, USA

68 34 Department of Biological Sciences, Florida International University, FL, USA

69 35 Agence Nationale des Parcs Nationaux, Libreville, Gabon

70 36 Institut de Recherche en Ecologie Tropicale, Libreville, Gabon

71 37 School of Natural Sciences, University of Stirling, Stirling, UK

72

73

74

75

76

77

78

79

80

81

82

Quantifying carbon dynamics in forests is critical for understanding their role in long-term climate regulation[1,2,3,4]. Yet little is known about tree longevity in tropical forests[3,5,6,7,8], a factor that is vital for estimating carbon persistence[3,4]. Here we calculate mean carbon age (the period that carbon is fixed in trees[7]) in different strata of African tropical forests using (i) growth-ring records with a unique timestamp accurately demarcating 66 years of growth in one site and (ii) measurements of diameter increments from the African Tropical Rainforest Observation Network (23 sites). We find that in spite of their much smaller size, in understory trees mean carbon age (74 years) is greater than in sub-canopy (54 years) and canopy (57 years) trees, and similar to carbon age in emergent trees (66 years). The remarkable carbon longevity in the understory results from slow and aperiodic growth as an adaptation to limited resource availability[9,10,11]. Our analysis also reveals that while the understory represents a small share (11%) of the carbon stock[12,13], it contributes disproportionally to the forest carbon sink (20%). We conclude that accounting for the diversity of carbon age and carbon sequestration among different forest strata is critical for effective conservation management[14,15,16], and for accurate modelling of carbon cycling[4].

Investing in carbon storage and sequestration represent important climate change mitigation strategies[3]. Forests have a potential to provide both long-lived carbon stocks[7,17] and long-term carbon sinks[1,2]. To successfully conserve forest carbon stock and increase forest carbon uptake, we must conserve carbon-rich forests and extend the forested land area[3], but decision makers and managers also need to understand the long-term behaviour of carbon within forests[1,2,3]. Critical questions are: (i) how long does the carbon persist, and (ii) where does it stay longest in the system? Carbon residence time is a direct function of tree longevity[3,7,17], but attempts to estimate tree age in tropical rainforests are relatively scarce and often highly contested[5,6,7,8]. Estimating the ages of the oldest trees in tropical forest stands is particularly subject to debate. While some authors claim that broadleaved trees in the tropics may reach ages of 1000 years or older[8,18], others estimate maximum ages of not more than 600 years[5,6]. Furthermore, the oldest carbon in the system is often assumed to be located in large trees[8]. Canopy and emergent trees contain a large proportion of the stand-level biomass[12,14] but large trees alone may not represent well the entire forest in terms of growth rates, tree lifespan and carbon persistence[7]. Canopy species grow faster[19], but there is a general trade-off between

4

growth and lifespan in organisms[9,20]. Therefore, long-term carbon storage and sequestration in tropical

rainforests may substantially depend on smaller trees too.

Here, we take advantage of a remarkable rediscovery of a historic forest inventory plot to probe the age

structure of African rainforests in a way that has not been possible to date. The Nkulapark plot was

established in 1948 in the southwest of the Democratic Republic of the Congo (Supplementary Fig.1). A

total of 6315 trees with diameter on breast height (DBH) >=5cm were tagged and DBH was measured

annually for 9 years. In 2014, we rediscovered and measured 450 surviving tagged trees, of which 55 were

selected to measure growth ring series. We used the grown-in iron nail as a 1948 timestamp, giving accurate

estimates of the DBH growth rate (in mm yr^{-1}) and the rate of growth-ring formation (number of rings per

year) over a 66 year period for each tree (Fig.1, Supplementary Table 1). The age of each individual tree (in

years) was calculated as the total number of rings from pith to bark, divided by the rate of growth-ring

formation (number of rings per year) (Fig.1, Fig.2). We used the five-class Crown Illumination Index of

Dawkins & Field (hereafter CII)[21,22] to compare growth patterns and tree age among the different rainforest

strata: understory (CII=1), sub-canopy (CII=2,3), canopy (CII=4) and emergent stratum (CII=5). Understory

trees receive no direct light, sub-canopy trees receive lateral light, canopy and emergent trees receive vertical

light (Fig.3a).Supplementary analyses show that the rediscovered Nkulapark tree dataset is adequate to

compare age differences between forest strata (Supplementary Fig.2, Supplementary Fig.3, Supplementary

Discussion).

We find that the age of the 55 Nkulapark trees with growth-ring series ranges between 129 and 452 years

(Fig.2, Supplementary Table 1). There is no clear linear relationship between tree age and their DBH

(p=0.082, Fig.2a). Understory trees (CII=1) do not differ significantly in age from canopy and emergent trees

(CII=4 or 5) (p=0.254, boxplot at the right of Fig.2b), while trees in sub-canopy classes (CII=2 or 3) are

slightly younger than trees in both the understory and the canopy. Despite their small size, understory trees

(CII=1) can be surprisingly old. One Microdesmis puberula (TreeID=3545) has an estimated age of 329

years, with a DBH of just 156 mm (Supplementary Table 1).

To test if our findings hold true in a wider geographic context, we compared growth and age patterns among
the different forest strata in 23 Central African permanent forest inventory plots[1] (Fig.3, Table 1,
Supplementary Fig.1 and Supplementary Table 2). Selected plots had a similar species composition as the
Nkulapark. Plots are demarcated rectangles or squares of median size 1 ha where each tree is mapped, tagged
and measured according to standard protocols[1,2]. DBH of each tree with DBH>= 10 cm was measured at
least twice. Small trees that grew larger than 10cm during the monitoring period were recorded as recruits.
Trees that died were recorded. We used repeated diameter measurements to estimate the growth rate of each
individual tree. We estimated tree age by dividing the final diameter (mm) by the growth rate (mm yr^{-1}),
assuming a constant growth rate over the lifetime of a tree[7]. We evaluated the robustness of this age
estimation method using the rediscovered Nkulapark trees as a reference (Supplementary Fig.4).
Uncertainties are due to relatively short plot monitoring periods (average 9 years), yielding negative or zero
growth rates for 9.7% of the trees. To avoid unrealistic tree age estimates, we replaced slow growth rates by
a 'minimum allowed growth rate', defined as the xth percentile of the growth rate distribution within each CII
class. Sensitivity analysis showed that x=25 returned a realistic tree age distribution for our dataset
(Supplementary Table 3, Supplementary Discussion). Further analysis suggests that x may be lower if
monitoring periods are longer. Finally, we estimated tree-level mean carbon age as the average age of each
year ring, weighted by the carbon content of the ring[7], with a year ring sequence deduced from the growth
rate.

The mean tree age for the 23 plots across the Congo Basin ranged between 131 and 284 years, with an
overall mean of 229 years (95% bootstrapped confidence intervals: 212-244 years) (Table 1). Mean tree age
in the understory (CII=1) is estimated to be 262 years, which is significantly older than the overall mean
(p<0.001) and older than the mean age of the sub-canopy (CII=3, 187 years, p<0.001), the canopy (CII=4,
194 years, p<0.001) and emergent classes (CII=5, 221 years, p=0.021) (Table 1). Furthermore, mean carbon
age at the tree level is 65 years (95% CI: 61-70). Carbon stored in the understory trees (CII=1) is estimated to
be on average 74 years (69-79), which is significantly older than the overall mean (p<0.001) and older than
carbon stored in the sub-canopy (CII=3, 54 years, p<0.001) and the canopy (CII=4, 57 years, p=0.001).

166 However, the difference between mean carbon age in the understory (CII=1) versus the emergent class

167 (CII=5, 66 years) is not significant (p=0.086) (Fig.3b and Table 1).

168

169 For each forest stratum within each plot, we calculated above-ground biomass-carbon stock (AGC-stock, in

170 Mg C ha^{-1}) and the AGC-sink (Mg C ha^{-1} yr^{-1}) using standard methods[1,2] (Table 1). The AGC-stock

171 represents the carbon reservoir in the system while the AGC-sink represents the net change, calculated as

172 AGC-productivity (additions to the system from tree growth) minus AGC-mortality (losses)[17]. The mean

173 AGC-stock in the understory (CII=1) is 19 Mg C ha^{-1}, which is 11% of the total plot-level AGC-stock (Table

174 1). The mean AGC-sink in the understory (CII=1) is 0.21 Mg C ha^{-1} yr^{-1} (Fig.3c), which represents 21% of

175 the plot-level AGC-sink. In contrast, the sub-canopy classes (CII=2 and 3) together contribute about 24% to

176 the AGC-stock, but nothing to the AGC-sink (-0.01 Mg C ha^{-1} yr^{-1}). The understory thus contributes

177 disproportionally to carbon sequestration, considering its relatively small share in the stock, and compared to

178 the limited contribution of the sub-canopy classes.

179

180 **Discussion**

181

182 Results from both the Nkulapark dataset (Fig.2) and the 23 inventory plots (Fig.3, Table 1) show that

183 understory (CII=1) and emergent (CII=5) trees are on average older than sub-canopy trees (CII=3). This

184 pattern can be explained by differences in species composition[15]. Understory 'specialist species' maintain

185 low growth rates for long periods, resulting in relatively small DBH at older age. Their adaptations allow

186 them to survive in the understory without the need to invest in rapid growth. The sub-canopy classes (CII=2

187 and 3) are populated with suppressed 'canopy specialists' that survived a recruitment stage but didn't reach

188 the canopy yet. These trees are relatively young (Fig.3) and they experience limited light conditions,

189 resulting in mortality rates equaling productivity rates (Table 1). Canopy and emergent trees (CII= 4 and 5

190 respectively) are canopy specialists that have been able to grow rapidly for long periods[23]. This is in line with

191 ref.[19] who show that growth rates in emergent trees are high and increase continuously. To test the

192 assumption that high tree and carbon age in the understory may be due to a difference in species

193 composition, we classified species as (i) understory specialists, (ii) non-specialists and (iii) canopy specialists

7

194 (Supplementary Discussion). This confirmed that understory specialists are on average smaller (p<0.001) but

195 older (p=0.003) than canopy specialists (Supplementary Table 4).

196

197 Furthermore, the Nkulapark dataset shows that there is a significant negative relationship between tree age

198 and growth-ring formation rate (Fig.2b). 91% of the trees in the dataset did not form a growth-ring every

199 year, suggesting an aperiodic growth pattern (shifts of growth to dormancy and back do not occur annually).

200 This aperiodic growth pattern is more prominent in understory trees, which formed fewer growth rings (0.36

201 rings per year) than canopy and emergent trees (0.61 rings per year) (p=0.01; boxplots at the top of Fig.2b).

202 Aperiodic growth patterns translate into significantly slower long-term growth rates: understory trees (CII=1)

203 have a mean DBH growth rate of 1.52 mm yr^{-1} versus 4.99 mm yr^{-1} in emergent trees (p<0.001) (Table 1).

204 The observed differences in growth periodicity (Fig.2b), growth rates (Table 1) and age patterns (Fig.3)

205 among the different forest strata are most likely a result of differences in survival mechanisms which are a

206 function of resource availability[11,24, 25] (Supplementary Discussion).

207

208 Our data show that growth and age distribution of tropical trees in mixed lowland rainforests is complex.

209 Large canopy trees are among the oldest in the rainforest, as suggested by several authors[8], but as they

210 obtained their size and position by maintaining fast growth rates[19], they are not significantly older than slow-

211 growing small understory specialists (Fig.2, Fig.3, Table 1). Furthermore, while large canopy trees represent

212 the largest share of the carbon stock[12,13,14], they suffer most during drought periods[26]. In comparison,

213 understory trees represent a smaller carbon capital but they are less vulnerable to drought and contribute

214 disproportionally to carbon sequestration. As such, the understory provides long-term stability in forest

215 carbon cycling. Furthermore, the understory is more diverse than the canopy in terms of species

216 composition[14,15,16]. Therefore, we recommend quantifying forest ecosystem services by considering forests as

217 a whole, with all forest strata providing specific services[16]. This is important in Central Africa, where the

218 demand for fuelwood and charcoal could severely affect the understory if only large trees were to be

219 protected[14,27].

220

221   Finally, our results suggest that care is required with large-scale modelling of forest carbon accumulation

222   potential and responses to different climate change scenarios[4]. There are two hypothesised responses to

223   increasing atmospheric CO_2 concentrations, possibly explaining the long-term observed AGC-sink in tropical

224   forests[1,2]: (i) big trees increase their asymmetric competition benefit to the detriment of the rest of the stand,

225   or (ii) suppressed trees do best, as they are closer to their light compensation point[17,28]. Our results show that

226   both scenarios occur in forest stands, with the understory (CII=1), the canopy (CII=4) and the emergent

227   (CII=5) classes contributing to carbon sequestration, while the sub-canopy classes (CII=2 and 3) do not

228   contribute. Forest and carbon cycle models will need to account for the diversity of carbon age and carbon

229   sequestration potential among the different forest strata. Recent studies have found that forest structure can

230   be predicted from the characteristics of canopy trees[13,14], but our results suggest that temporal dynamics

231   differ between forest strata. The long-term persistence of function depends on smaller trees too, which

232   compared to their stature contribute disproportionately heavily to long-term carbon storage, sequestration,

233   and climate resilience.

234

References

236   1.   Lewis, S. L. et al. Increasing carbon storage in intact African tropical forests. Nature **457,** 1003–1006

237   (2009).

238   2.   Brienen, R. J. W. et al. Long-term decline of the Amazon carbon sink. Nature **519,** 344–348 (2015).

239   3.   Körner, C. A matter of tree longevity. Science **355,** 130–131 (2017).

240   4.   Galbraith, D. et al. Residence times of woody biomass in tropical forests. Plant Ecol. Divers. **6,** 139–

241   157 (2013).

242   5.   Brienen, R. J. W., Schöngart, J. & Zuidema, P. A. Tree Rings in the Tropics : Insights into the

243   Ecology and Climate Sensitivity of Tropical trees. in Tropical Tree Physiology (eds. Goldstein, G. &

244   Santiago, L. S.) **6,** (2016).

245   6.   Worbes, M. One hundred years of tree-ring research in the tropics – a brief history and an outlook to

246   future challenges. Dendrochronologia **20,** 217–231 (2002).

247   7.   Vieira, S. et al. Slow growth rates of Amazonian trees: Consequences for carbon cycling. Proc. Natl.

248   Acad. Sci. **102,** 18502–18507 (2005).

249 8. Chambers, J. Q., Higuchi, N. & Schimel, J. P. Ancient trees in amazonia. Nature **391,** 135–136

250   (1998).

251 9. Bigler, C. Trade-Offs between growth rate, tree size and lifespan of mountain pine (Pinus Montana)

252   in the swiss national park. PLoS One **11,** 1–18 (2016).

253 10. Kleczewski, N. M., Herms, D. A. & Bonello, P. Effects of soil type, fertilization and drought on

254   carbon allocation to root growth and partitioning between secondary metabolism and ectomycorrhizae

255   of Betula papyrifera. Tree Physiol. **30,** 807–817 (2010).

256 11. Sass-Klaassen, U. Tree physiology: Tracking tree carbon gain. Nat. Plants **1,** 15175 (2015).

257 12. Bastin, J.-F. et al. Seeing Central African forests through their largest trees. Sci. Rep. **5,** 1–8 (2015).

258 13. Bastin, J.-F. et al. Pan-tropical prediction of forest structure from the largest trees. Glob. Ecol.

259   Biogeogr. **in press,** (2018).

260 14. Lutz, J. A. et al. Global importance of large-diameter trees. Glob. Ecol. Biogeogr. **27,** 849–864

261   (2018).

262 15. Memiaghe, H. R., Lutz, J. A., Korte, L., Alonso, A. & Kenfack, D. Ecological Importance of Small-

263   Diameter Trees to the Structure, Diversity and Biomass of a Tropical Evergreen Forest at Rabi,

264   Gabon. PLoS One **11,** 1–15 (2016).

265 16. Burton, J. I., Ares, A., Olson, D. H. & Puettmann, K. J. Management trade-off between aboveground

266   carbon storage and understory plant species richness in temperate forests. Ecol. Appl. **23,** 1297–1310

267   (2013).

268 17. Lloyd, J. & Farquhar, G. D. The CO2 dependence of photosynthesis, plant growth responses to

269   elevated atmospheric CO2 concentrations and their interaction with soil nutrient status . I . General

270   principles and forest ecosystems. Funct. Ecol. **10,** 4–32 (1996).

271 18. Laurance, W. F. et al. Inferred longevity of Amazonian rainforest trees based on a long-term

272   demographic study. For. Ecol. Manage. **190,** 131–143 (2004).

273 19. Stephenson, N. L. et al. Rate of tree carbon accumulation increases continuously with tree size.

274   Nature **507,** 90–93 (2014).

275 20. Wright, S. J. et al. Functional traits and the growth — mortality trade-off in tropical trees. Ecology

276   **91,** 3664–3674 (2013).

10

277 21. Synnott, T. J. A manual of permanent plot procedures for tropical rainforests. Tropical forestry

278   papers **14,** (1979).

279 22. Dawkins, H. C. & Field, D. R. B. A long-term surveillance system for British woodland vegetation.

280   Oxford Forestry Institute Occasional Papers **1,** (1978).

281 23. Hall, J. S., Harris, D. J., Medjibe, V. P. & Ashton, M. S. The effects of selective logging on forest

282   structure and tree species composition in a Central African forest: Implications for management of

283   conservation areas. For. Ecol. Manag. **183,** 249–264 (2003).

284 24. Couralet, C., Van den Bulcke, J., Ngoma, L. M., Van Acker, J. & Beeckman, H. Phenology in

285   functional groups of Central African trees. J. Trop. For. Sci. **25,** 361–374 (2013).

286 25. Vico, G., Dralle, D., Feng, X., Thompson, S. & Manzoni, S. How competitive is drought

287   deciduousness in tropical forests? A combined eco-hydrological and eco-evolutionary approach.

288   Environ. Res. Lett. **12,** 65006 (2017).

289 26. Bennett, A. C., McDowell, N. G., Allen, C. D. & Anderson-Teixeira, K. J. Larger trees suffer most

290   during drought in forests worldwide. Nat. Plants **1,** 15139 (2015).

291 27. FAO. *The charcoal transition : greening the charcoal value chain to mitigate climate change and*

292   *improve local livelihoods.* (Food and Agriculture Organization of the United Nations, 2017).

293 28. Lewis, S. L., Malhi, Y. & Phillips, O. L. Fingerprinting the impacts of global change on tropical

294   forests. Philos. Trans. R. Soc. B Biol. Sci. **359,** 437–462 (2004).

295 29. Hietz, P. A simple program to measure and analyse tree rings using Excel, R and SigmaScan.

296   Dendrochronologia **29,** 245–250 (2011).

297 30. Benjamini, Y. & Hochberg, Y. Controlling the False Discovery Rate: A Practical and Powerful

298   Approach to Multiple Testing. J. R. Stat. Soc. Ser. B **57,** 289–300 (1995).

299

Correspondence

301 Correspondence and requests for materials should be addressed to W.H. (whubau@gmail.com).

302

303

304

Acknowledgments

Author contributions

W.H., T.D.M., J.V.d.B., J.V.A. and H.B. conceived and designed the study. T.D.M. and B.A.I. coordinated collection of Nkulapark data and wood cores. T.D.M. and J.V.d.B. measured growth ring series. W.H. carried out the data analysis and wrote the paper. S.L.L., O.L.P., T.R.B. and Y.M. conceived the AfriTRON

332 forest census network programmes and the Forestplots.net database, and most co-authors helped collecting

333 AfriTRON forest census data. S.L.L., B.S., S.B., A.C.S., W.H., T.S. and L.W.W. coordinated forest plots

334 data collection. M.J.P.S., G.L.G., S.L.L., O.L.P., T.R.B. and G.P. contributed tools to analyze and curate

335 data. All co-authors commented on or approved the manuscript.

336

Competing financial interests

338 The authors declare no competing financial interests.

339

Figure legends

341

342 **Figure 1 Example of a wood core (Greenwayodendron suaveolens, TreeID=765) showing the 1948 nail**

343 **trace.** The image at the top shows the full core. White lines indicate growth-ring boundaries, numbers

344 indicate growth-rings (counted from bark to pith), black arrows indicate important years. The bark to the

345 right of the figure indicates the year of sampling (2014). The dark discoloration in growth-rings 26 to 35 was

346 caused by oxidates from the iron nail that were transported up and down in damaged vessels and fibers. The

347 right border of the discoloration accurately marks the start of the year 1948. There are 25 rings between the

348 bark and the 1948 nail trace, suggesting that this individual needed on average 2.6 years to form a ring.

349 Using this rate for the 53 rings that were formed before 1948, we find that the first ring in the core was

350 probably formed around 1811. The location of the pith is indicated by the black lines to the left, which

351 follow the direction of the wood rays[29]. This shows that the distance from the pith to the first ring boundary

352 in the core is about 11 mm. When using the average ring width of rings 78 to 68, we estimate that 7 rings are

353 missing. As such, this individual would be about 224 years old. The three close-ups at the bottom illustrate

354 wood anatomical details used to identify growth-ring boundaries (indicated by white triangles). Ring

355 boundaries in this species are demarcated by distended wood rays and flattening of the fibers. Black scale

356 bars cover 0.2 mm.

357

Figure 2 Variation in tree age inferred from growth-ring patterns in 55 trees where nail traces accurately mark the year 1948. Panel (a) shows the relation between tree age and DBH. Panel (b) shows the relation between tree age and the growth-ring formation rate (number of rings per year) between 1948-2014. In both panels, p-values of simple linear regression models are given in red. Brown dots represent understory individuals (Crown Illumination Index =1), grey dots represent sub-canopy individuals (CII=2 and 3), blue dots represent canopy and emergent trees (CII=4 and 5). Boxplots show the first quartile, the median value and the third quartile of the tree age distribution (vertical axis, boxplots to the right) and of the variables in the x-axis (horizontal boxplots at the top of the panels). P-values under boxplots resulted from two-sided Wilcoxon rank-sum tests. Outliers are marked with open circles.

Figure 3 Estimation of mean carbon age and AGC-sink per crown illumination category, for 23 permanent inventory plots in Central Africa. The 450 rediscovered Nkulapark trees were treated as an additional plot to estimate distributions of mean carbon age. Panel (a) illustrates the Crown Illumination Index (CII) developed by Dawkins and Field (ref.[22]), with yellow arrows indicating reception of sunlight (drawing modified from ref.[21]). Understory trees (brown, CII=1) receive no direct sunlight, sub-canopy trees (grey) receive lateral (CII=2) or restricted vertical (CII=3) light, canopy trees (blue, CII=4) are almost completely exposed to vertical light and emergent trees (blue, CII=5) have a crown that is completely exposed to vertical and lateral light. Boxplots in panels (b) and (c) show the distribution of plot-level mean carbon age and plot-level AGC-sink per CII class. Boxplots represent the 25 % quartile, the median value and the 75 % quartile of the plot-level average ages. Outliers are marked with open circles. Comparison among CII classes was performed with Dunn's rank-sum test using the Benjamini-Hochberg adjustment for multiple comparisons [30]. The grey dotted line shows the overall (plot-level) average age.

Tables

metric	All trees	CII 1	CII 2	CII 3	CII 4	CII5	p-value
Tree age (yr)	**229** (212-244)	**262** (243-282)	**210** (196-223)	**187** (170-204)	**194** (175-212)	**221** (192-250)	0.021
Mean carbon age (yr)	**65** (61-70)	**74** (69-79)	**60** (55-64)	**54** (49-59)	**57** (51-63)	**66** (57-75)	0.086
AGC-prod (MgC ha-1 yr-1)	**3.1** (2.83-3.41)	**0.47** (0.4-0.56)	**0.53** (0.42-0.67)	**0.35** (0.27-0.43)	**0.9** (0.69-1.15)	**0.82** (0.63-1)	0.015
AGC-mort (MgC ha-1 yr-1)	**2.05** (1.66-2.48)	**0.26** (0.19-0.36)	**0.62** (0.49-0.76)	**0.28** (0.18-0.38)	**0.61** (0.41-0.85)	**0.27** (0.07-0.61)	0.058
AGC-sink (MgC ha-1 yr-1)	**1.05** (0.63-1.5)	**0.21** (0.09-0.33)	**-0.08** (-0.23-0.05)	**0.07** (-0.06-0.2)	**0.3** (0-0.59)	**0.55** (0.26-0.79)	0.011
AGC-stock (Mg C ha-1)	**177** (159-198)	**19** (15-23)	**26** (21-31)	**17** (12-22)	**58** (42-74)	**59** (46-75)	<0.001
stem density (stems ha-1)	**428** (392-465)	**194** (165-228)	**112** (94-130)	**38** (33-44)	**59** (46-70)	**25** (19-31)	<0.001
DBH (mm)	**313** (291-338)	**161** (154-168)	**235** (222-250)	**299** (273-326)	**435** (397-469)	**700** (644-760)	<0.001
DBH growth (mm yr-1)	**2.38** (2.17-2.63)	**1.51** (1.35-1.69)	**2.16** (1.96-2.38)	**2.98** (2.69-3.31)	**4.03** (3.71-4.34)	**4.99** (4.32-5.68)	<0.001
wood density (g cm-3)	**0.59** (0.56-0.61)	**0.64** (0.62-0.65)	**0.61** (0.6-0.63)	**0.59** (0.56-0.61)	**0.59** (0.56-0.61)	**0.57** (0.53-0.61)	0.006
ratio evergreen:deciduous	**3.27** (2.85-3.71)	**4.72** (3.86-5.59)	**4.61** (2.76-7.85)	**3.62** (2.78-4.6)	**3.03** (2.09-4.22)	**1.78** (0.88-3.43)	<0.001
proportion evergreen trees (%)	**55** (52-57)	**56** (52-59)	**55** (51-59)	**56** (52-61)	**51** (46-56)	**44** (37-52)	0.01
proportion deciduous trees (%)	**18** (16-20)	**14** (12-17)	**19** (16-22)	**21** (17-25)	**26** (21-31)	**35** (28-41)	<0.001

Table 1 Estimation of plot-level mean tree age, mean carbon age, aboveground carbon sink (AGC-sink), AGC-stock and leaf habit per crown illumination category, for 23 permanent forest plots. The 450 rediscovered Nkulapark trees were treated as an additional plot for estimation of tree age and mean carbon age (first two rows). All metrics were averaged per plot and per CII class. Mean values are given in bold, 95% confidence intervals are given between brackets. Components of the AGC-sink are AGC-productivity and AGC-mortality. Components of AGC-stock are diameter (DBH), wood density and stem density. Comparison among CII classes was performed with Dunn's rank-sum test using the Benjamini-Hochberg adjustment for multiple comparisons[30]; the reported p-values compare CII1 and CII5.

Online Methods

Site description. The Nkulapark is a phenology and tree-growth monitoring plot covering 174 ha within the Luki Man and Biosphere reserve, located in the southern Mayumbe mountains in the Democratic Republic of the Congo[24] (Supplementary Fig.1). The region experiences a humid tropical climate with a dry season between mid-May and mid-October and a short dry season from mid-December to mid-February. Yearly precipitation ranges from 649 mm to 1853 mm with a mean precipitation of 1173 mm. Temperature ranges between 19 °C and 30 °C with a mean temperature of 25.5 °C [24]. The Nkulapark is situated almost entirely in a catchment with a valley and a ridge and includes several microclimatic conditions. The semi-deciduous lowland forest consists of (i) mature forest dominated by Prioria balsamifera, (ii) old regenerating forest dominated by Terminalia superba, (iii) mixed-species mature forest and (iv) modified forest patches[31,32].

Nkulapark plot design in 1948. The Nkulapark was established and managed by the Institut National pour *l'Etude Agronomique du Congo Belge* (INEAC), which was later renamed *Institut National pour l'Et*ude et la Recherche Agronomique en R.D.Congo (INERA, http://www.inera-drc.org). The person in charge of the tagging and the measurements was Léon Toussaint, who worked as a botanist in the Luki reserve between 1946 and 1952[33]. The planning of the plot was first announced in the INEAC-Luki annual report of 1946[34]. A total of 29.2 km of observation paths were cut in the forest in 1947, following the contour lines of the Nkula river valley (Supplementary Fig.1)[31]. A total number of 6315 trees were tagged by the end of 1947[31], so we assume that first wood formation after tagging occurred during the wet season that started in October 1948. Tree selection was performed by randomly selecting trees from the pool of trees > 5 cm DBH in 1948. The Nkulapark area was mapped, showing the locations of the largest tagged trees. From 1948 to 1957 yearly diameter measurements were performed on all tagged trees[35]. Mortality events were recorded in the datasheets. Trees were measured at a height of 1.3 m and the point of measurement (POM) was indicated on the tree with a horizontal line of lead-based paint. For trees with buttresses or deformities, the POM was raised to a point high enough to avoid the irregularities interfering with diameter measurements at subsequent censuses. For trees with extremely high buttresses, diameters were estimated. For the same 6315 trees, weekly phenology observations were recorded. Phenological observations were done for leaf habit,

16

432   flowering, fruiting and seed dissemination. The plot was abandoned in 1957 but the datasheets were kept in

433   the library of the INERA station in Luki and digitized in 2008[24] and 2014.

434

435   Rediscovering Nkulapark trees in 2014.Each of the original 6315 Nkulapark trees were labelled during the

436   first census in 1948 with a zinc number tag that was attached to the tree using an iron nail of 8 cm long. A

437   part of these trees were indicated on the original 1948 map. During a first prospective field campaign in

438   august 2014, this map was digitized and georeferenced with QGIS (QGIS development team, 2016) using

439   landmarks such as easily rediscovered trees, contour lines and observation paths that were still visible and

440   could be tracked with a Garmin 64s GPSmap (see Supplementary Fig.1). Based on this map, we pinpointed

441   the approximate location of 1521 individuals that were recorded as alive during the last census in 1957.

442   During a second field campaign in September- October 2014, these 1521 individuals were searched for. 450

443   of them were found alive, 16 were found dead and the remaining 1057 could not be relocated and were

444   assumed to be dead and rotten away, albeit some may have been missed (see Supplementary Fig.2,

445   Supplementary Fig.3, Supplementary Discussion for an in-depth analysis of survivorship rates). The original

446   1948 tree tags and nails of the rediscovered trees were either still present outside the trunk or detected inside

447   the tree using a metal detector (BHJS, Bounty Hunter, USA). Scars on the trunk indicated the presence of an

448   overgrown nail, and repelled number tags were sometimes found on or in the ground nearby the tree using

449   the metal detector. In most cases, the numbers on the tags were still readable. On 95% of the rediscovered

450   trees, the lead-based paint of the POM was still visible, allowing a representative DBH measurement.

451   Comparison of DBH, DBH growth rates and tree age distribution in the original dataset of Nkulapark trees

452   versus the dataset of rediscovered trees, showed that the rediscovered dataset is slightly biased towards

453   discovering slower-growing trees, but this bias affected both the classes of understory and canopy 'specialist'

454   species (Supplementary Fig.3). Hence, the rediscovered tree dataset is representative to compare growth and

455   age patterns among the different forest strata in the Nkulapark area.

456

457   Sampling Nkulapark trees in 2014. Wood samples for growth-ring analysis were taken from rediscovered

458   trees if following criteria were met : (a) the nail was still present in the wood, either totally grown-in or

459   partly sticking out of the trunk, (b) the exact position of the nail could be identified visually or with the metal

460 detector, (c) the nail was not overgrown by excessive wound tissue, buttresses or other deformities. As such,

461 increment cores or stem discs were taken near the nail for 58 of the rediscovered trees. For each sampled

462 tree, increment cores were taken a few centimetres above, below, to the left and to the right of the nail using

463 a 40cm Pressler bore. For each tree, two additional cores were taken at 120° from the nail trace along the

464 circumference of the tree. As such, 6 increment cores were available for each tree. This maximised the

465 chance of sampling the pith of the tree. To study and describe the reaction of the wood after tagging,

466 additional larger wood samples containing the nail were extracted from 30 trees using a saw and a chisel.

467

468 Visualizing and measuring growth-ring series. For each wood core, growth-ring series were visualized using

469 two imaging methods as described by ref.[36]: (i) first, density profiles were calculated from X-ray CT scans of

470 entire wood cores, then (ii) the cores were surfaced with a core microtome[37] and scanned using a flatbed

471 scanner (EPSON Perfection 4990 PHOTO). To obtain X-ray CT volumes, cores were scanned at 110 µm

472 resolution with the Nanowood CT facility from the Centre for X-ray Computed Tomography of Ghent

473 University (UGCT, www.ugct.ugent.be)[38], developed in collaboration with XRE (www.xre.be; now part of

474 the TESCAN ORSAY HOLDING a.s.). Reconstruction was performed with the Octopus software package

475 on a GeForce GPX 770 4GB GPU[38,39]. X-ray and flatbed scans were analysed using the toolchain for tree-

476 ring analysis described by De Mil et al. (ref. [36]). This toolchain semi-automatically indicates the growth-ring

477 boundaries and calculates growth-ring width series. Depending on the visibility of the growth-ring patterns,

478 either the X-ray or the flatbed scans were used to check growth-ring boundaries and measure growth-ring

479 widths. Growth-ring boundaries were distinguished using visual wood anatomical characteristics such as

480 distended rays, flattened fibers and terminal parenchyma bands[5,40,41]. For unclear ring boundaries,

481 microscopic thin sections were taken to study wood anatomy at high resolution using an Olympus BX60

482 microscope (Fig.1).

483

484 Detecting the 1948 nail trace. Discolorations or wound tissue formed as a reaction on the tagging were

485 visible in the cores taken near the nail. The surface of these stem discs was sanded to a few millimetres

486 above the nail and the anatomy was observed using an Olympus BX60 microscope. The nails were

487 remarkably well preserved inside the trees, probably due to cathodic protection of the iron by the zinc of the

18

488 tags. Hence, discolorations or wound tissue were visible in each of these samples. Discolorations were

489 recognizable as darkened tissue in otherwise light-coloured wood (Fig.1). Discolorations occurred in cells

490 that were formed before the nail was inserted, due to oxidation processes between the wood and the iron nail.

491 Water in vessels and fibers in the neighbourhood of the nail (especially those damaged by the nail) spread

492 these oxidates upwards and downwards. Therefore, the discolorations in these cells are also detectable on

493 samples that were taken a few centimetres under or above the nails. Vessels and fibers that were formed after

494 the tagging were not damaged, hence did not show discolorations. As such, the boundary of the discoloration

495 accurately serves as a timestamp indicating the year of tagging (1948). Furthermore, wound-induced

496 deformities occurred in the wood that was formed after the nail was inserted. This wound tissue is

497 characterized by increased woody productivity around the nail, forming a lump in the growth-rings that were

498 formed just after the nail was inserted. This lump formation is not present in the wood that was formed

499 before tagging.

500

501 Estimating tree age using growth rings and nail traces. Six cores were assessed for each tree. For some trees,

502 none of the cores contained the pith because (i) the tree radius exceeded the borer length or (ii) the pith was

503 eccentric and missed. In these cases, the core with the largest number of visible rings was used to estimate

504 the total number of growth-rings. The missing core length from the end of this core to the pith was estimated

505 using the intersection of three lines of ring boundaries marked along the rays, as described by ref.[29] (see

506 Fig.1 for an example). We estimated the number of rings in the missing core part by dividing the missing

507 core length by the average ring width of the 5 oldest rings of the sampled core. We tested the robustness of

508 this method by rerunning the analysis using the average growth rates of the 5, 10, 15 and 20 oldest rings. We

509 found that the overall average tree age and the trends observed in Fig.2 are not sensitive to varying the

510 method used to estimate the number of rings in the missing part of the core. The core with the clearest nail

511 trace was used to count the number of rings formed after the year of tagging (1948). We used the number of

512 growth-rings formed between 1948 (nail mark) and 2014 (cambium) as a reference to calculate the number

513 of years the individual needed to form one ring (years per ring). We then multiplied this ratio with the total

514 number of rings formed before 1948 to estimate the age of the tree (Fig.1 and Fig.2). Three individuals were

515   not used for analysis because the estimated missing core length of each core exceeded 20 cm. As such,

516   growth-ring series of 55 trees were retained (Supplementary Table 1).

517

518   Permanent forest inventory plots. To test if our findings hold true in a wider geographic context, we

519   estimated mean tree age and carbon age of the different forest strata in 23 Central African permanent forest

520   plots located in four different Central African countries (Cameroon, Gabon, Congo Brazzaville, D.R.Congo)

521   (Supplementary Fig.1 and Supplementary Table 2). Plots were selected if at least 65% of the trees belonged

522   to species that also occur in the Nkulapark. Furthermore, plots selected for analysis conformed to the

523   following criteria[1,2,42]: (1) plots had an actual plot area of ≥0.2 ha, (2) plots were georeferenced, (3) all trees

524   with DBH ≥100 mm were measured, (4) the majority of stems were identified to species level, (5) plots had

525   at least 2 censuses, (6) plots had a total monitoring length of ≥ 3 years, (7) plots were situated within

526   structurally intact, apparently mature forest (excluding young or open forests), (8) plots were free from major

527   human impacts, (9) plots were located at ≥50m from the anthropogenic forest edge, (10) altitude was below

528   1500 m.a.s.l., (11) mean annual air temperature was ≥20.0°C, (12) mean annual precipitation was ≥1000 mm

529   yr[-1], (13) plots were located in terra firme forest. For analysis purposes, plots smaller than 0.5 ha that were

530   within 1 km of each other and located in similar forest types were merged (i.e. the LME cluster). All selected

531   plots are part of the African Tropical Rainforest Observatory Network (AfriTRON; www.afritron.org). These

532   data are curated in the ForestPlots.net database[43], and subject to identical quality control and quality

533   assurance procedures. All calculations of plot data metrics described hereafter were performed using the R

534   statistical platform[44], version 3.2.1.

535

536   Estimating AGC-stock. For each tree and each census, Aboveground Biomass at the tree level (AGB, Mg

537   stem[-1]) was estimated using a published allometric equation for moist forests including terms for diameter

538   (DBH, mm), dry wood density (ρ, g cm^{-3}) and total tree height (H, m)[45] :

539    $$AGB = \frac{0.0673 \times (\rho \times (\frac{DBH}{10})^2 \times H)^{0.976}}{1000}$$ (formula 1).

540   Wood density values were derived from the dryad database (www.datadryad.org). Stems were matched to

541   species-specific wood density values or the mean values for the genus or family, following ref.[1] and[43].

20

542   Heights were calculated using a single height-diameter model (Weibull) for central African lowland terra

543   firme forests published by ref.[46], using commands implemented in the R-package BiomasaFP[47].

544   Aboveground Biomass-Carbon (referred to as AGC) is considered as 47% of the AGB following IPCC

545   recommendations[48]. For each individual tree in the plot dataset, AGC-stock was calculated as the mean of the

546   first and last censuses.

547

548   Estimating AGC-sink. For the calculation of AGC-sink, only the first and the last censuses were used for

549   each plot. First, AGC- productivity (Mg C stem^{-1} yr^{-1}) for each stem surviving the monitoring period, was

550   calculated as the difference between its total AGC at the end census minus the total AGC at the start census

551   of the interval, divided by the census interval length (yr). AGC-productivity for stems recruited during the

552   monitoring period (i.e. reaching DBH≥100 mm), was calculated in the same way, assuming DBH=0 mm at

553   the start of the interval. AGC-mortality for each tree that died during the monitoring period (Mg C tree^{-1} yr^{-1})

554   was calculated as the AGC at the start of the monitoring period, divided by the total monitoring length (yr).

555   AGC-productivity at the stand level (Mg C ha^{-1} yr^{-1}) was then calculated as the sum of tree-level productivity

556   estimates of all survivors and recruits. AGC-mortality at the stand level (Mg C ha^{-1} yr^{-1}) was calculated as the

557   sum of tree-level mortality estimates of all dead trees in the subset. We corrected for unobserved components

558   of biomass growth and mortality due to census interval length effects, as discussed by ref.[2], ref.[49] and ref.[50].

559   A method to correct productivity and mortality rates for these uncertainties was developed by ref.[49] and

560   applied by ref.[2]. This correction accounts for (i) trees that recruit and die within the same interval (i.e.

561   unobserved recruits) and (ii) growth of trees that grow and die within the interval (i.e. unobserved biomass

562   growth from mortality, which is not recorded because dead trees are not measured). As such, for each census

563   interval, we calculated unobserved recruitment and unobserved mortality components (Mg ha^{-1} yr^{-1}) using

564   the formulas proposed by ref.[49] and both components were added to both the AGC-productivity and AGC-

565   mortality estimates. Estimates of the unobserved biomass components usually accounted for less than 3% of

566   the total AGC-productivity and AGC-mortality. Finally, the AGC-sink was calculated as stand-level AGC-

567   productivity minus AGC-mortality. Commands to calculate AGC-stock and AGC-sink are implemented in

568   the BiomasaFP R package [47].

569

570   Tree age inferred from DBH growth rates in permanent inventory plots. For each tree within the permanent

571   forest inventory plots, we estimated the age by dividing the DBH (mm) in the final census with the DBH

572   growth rate (mm yr^{-1}) of the tree itself. For each tree, we averaged the DBH growth rate over all census

573   intervals preceding the last census. This method uses the actual growth rate of each tree, which is accurate

574   for healthy trees but returns unrealistic age estimates for trees with (i) slightly negative growth rates, (ii) zero

575   growth rates or (iii) very slow growth rates. Such slow growth rates may be recorded in all DBH classes.

576   First, slow growth rates in large DBH classes may occur when a tree is diseased or at the end of its life

577   (senescence). These growth rates may not be representative for the total lifespan of these trees. Secondly,

578   small growth rates may be recorded for small suppressed trees if their growth is so slow that it cannot be

579   recorded with sufficient precision using standard census procedures. Hence, these growth rates are replaced

580   by growth rates that are comparably small but yield a realistic tree age estimate. As such, we chose a

581   'minimum allowed growth rate' per CII class, following ref.[7]. We calculated the minimum allowed growth

582   rate for each CII class as the 25th percentile (=first quartile) of the growth rate distribution within the CII

583   class. For each tree with a growth rate slower than the minimum allowed rate, we replaced the growth rate by

584   the minimum allowed growth rate of the CII class. We conducted a sensitivity analysis to check how results

585   vary when varying the minimum allowed growth rate: we reran the analysis using the 10th, 15th, 20th, 25th and

586   30th percentile of the growth rate distribution within each CII class as a minimum allowed growth rate

587   (Supplementary Discussion and Supplementary Table 3). We used the average tree age in the dataset of 450

588   rediscovered Nkulapark trees as a reference to evaluate the tree-age estimation method based on DBH

589   growth rates (Supplementary Figure 4).

590

591   Mean carbon age. As a tree grows, it increasingly stores more carbon. Carbon near the bark of the tree is

592   younger than carbon in the pith. As such, mean carbon age of a tree does not equal total tree age. We

593   calculated mean tree-level carbon age using the same formula as ref.[7]:

594   $mean\ carbon\ age = \frac{\sum_{i=1}^{n}(C_i \times A_i)}{\sum_{i=1}^{n}(C_i)}$ (formula 2),

595   with:

596   C_i = carbon content of the ith ring (kg),

597   A_i = age of the ith ring (yr),

598   n   = nr of rings.

599

600   The carbon content of the ith ring is calculated as the carbon content of a tree with the DBH of ring i minus

601   the carbon content of a tree with the DBH of ring i-1. To estimate carbon age in trees without measured

602   growth-ring series (permanent inventory plots), we used the final DBH and the DBH growth rate (in mm yr[-]

603   [1]) to deduce a year-ring pattern, assuming that the growth rate was constant over the lifetime of the tree.

604

605   Classification of tree species and statistical analysis. We used the Nkulapark phenology data published by

606   ref.[24] to classify tree species as evergreen or deciduous. To distinguish between understory, sub-canopy,

607   canopy and emergent trees in the Nkulapark and the permanent forest plots, we used the Crown Illumination

608   Index (CII) of Dawkins & Field (ref.[22]). Fig.3 illustrates the 5 classes with a drawing modified from ref.[21].

609   The Crown Illumination Index was recorded in 23 of the selected permanent inventory plots. In each plot

610   where the index was recorded, each tree was attributed to one of the CII classes. The index was attributed in

611   the field, mostly during one census and mostly by a single person. We estimated mean tree age, mean carbon

612   age, mean AGC-stock and mean AGC-sink for each of the CII classes in each plot where the index was

613   recorded. None of the metrics reported in Table 1 meet the criterion of homogeneity of variances (Bartlett

614   test). Therefore, differences among the CII classes were tested using the non-parametric Dunn's rank-sum

615   test. To avoid the multiple comparison problem, we used the Benjamini-Hochberg p-value adjustment[30]

616   ('dunn.test' package in R[44]).

617

618   Data availability. The input data and R-scripts to generate the figures and tables are available for download

619   using the following private link : https://figshare.com/s/06c793575d3b52ef5574. Images of wood cores are

620   available using the following link : https://figshare.com/s/e6101fe7d330f8ea140a . This folder also contains

621   all annotation documents needed to visualize growth ring boundaries on the wood samples (please consult

622   the README document for guidelines). Wood samples used to conduct this analysis are stored in the

623   Tervuren xylarium

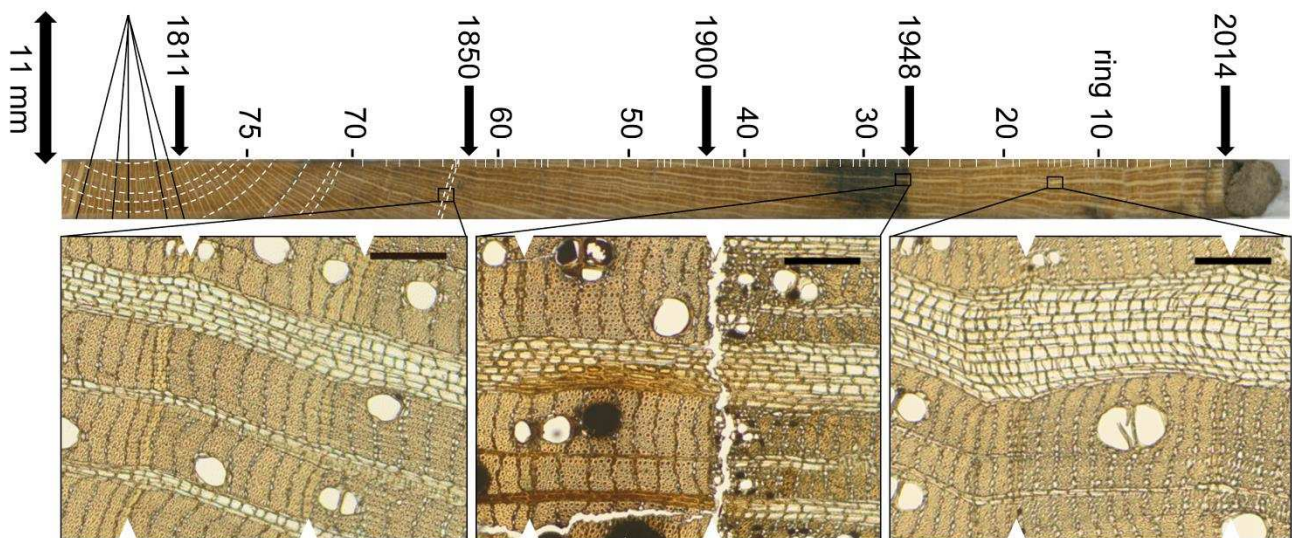624   (http://www.africamuseum.be/collections/browsecollections/naturalsciences/earth/xylarium). These samples

may be studied, within the Tervuren xylarium, upon request addressed to the curator H.B.

(hans.beeckman@africamuseum.be) or the corresponding author W.H. (whubau@gmail.com).

References (methods only)
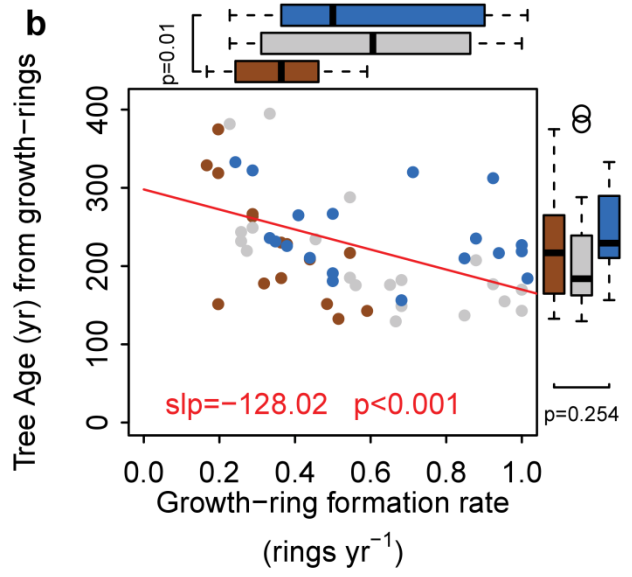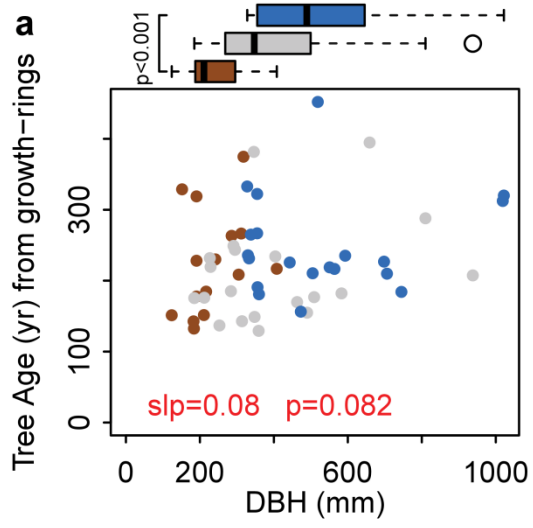
31.   INEAC. Rapport Annuel INEAC-Luki. (1947).

32.   Coppieters, G. Inventaris van het archief van de Rijksplantages en de Regie der Plantages van de Kolonie, het Nationaal Instituut voor de Landbouwkunde in Belgisch-Congo en de Documentatiedienst voor Tropische Landbouwkunde en Plattelandsontwikkeling 1901-1999. (2013).

33.   Académie Royale des Sciences d'outre-mer. *Biographie Coloniale Belge/Biographie Belge d'Outre-Mer, Tome IX.* (2015).

34.   INEAC. Rapport Annuel INEAC-Luki. (1946).

35.   INEAC. Rapport Annuel INEAC-Luki. (1948).

36.   De Mil, T., Vannoppen, A., Beeckman, H., Van Acker, J. & Van Den Bulcke, J. A field-to-desktop toolchain for X-ray CT densitometry enables tree ring analysis. Ann. Bot. **117,** 1187–1196 (2016).

37.   Gärtner, H. & Nievergelt, D. The core-microtome: A new tool for surface preparation on cores and time series analysis of varying cell parameters. Dendrochronologia **28,** 85–92 (2010).

38.   Dierick, M. et al. Recent micro-CT scanner developments at UGCT. Nucl. Instruments Methods Phys. Res. Sect. B Beam Interact. with Mater. Atoms **324,** 35–40 (2014).

39.   Vlassenbroeck, J. et al. Software tools for quantification of X-ray microtomography at the UGCT. Nucl. Instruments Methods Phys. Res. Sect. A Accel. Spectrometers, Detect. Assoc. Equip. **580,** 442–445 (2007).

40.   Worbes, M. Tree-Ring Analysis. Encycl. For. Sci. 586–599 (2004).

41.   Tarelkin, Y. et al. Growth-ring distinctness and boundary anatomy variability in tropical trees. IAWA J. **37,** 275–294 (2016).

42.   Phillips, O. & Baker, T. Field manual for plot establishment and remeasurement - RAINFOR. Rainfor 22 (2009). doi:10.13140/RG.2.1.1735.7202

43.   Lopez-Gonzalez, G., Lewis, S. L., Burkitt, M. & Phillips, O. L. ForestPlots.net: A web application and research tool to manage and analyse tropical forest plot data. J. Veg. Sci. **22,** 610–613 (2011).

653   44.   R Development Core Team. R: A language and environment for statistical computing. (2008).

654   45.   Chave, J. et al. Improved allometric models to estimate the aboveground biomass of tropical trees.

655   Glob. Chang. Biol. **20,** 3177–3190 (2014).

656   46.   Feldpausch, T. R. et al. Tree height integrated into pantropical forest biomass estimates.

657   Biogeosciences **9,** 3381–3403 (2012).

658   47.   Lopez-Gonzalez, G., Sullivan, M. & Baker, T. BiomasaFP package. Tools for analysing data

659   downloaded from ForestPlots.net. R package version 1.1. Available at

660   http://www.forestplots.net/en/resources. (2015).

661   48.   Aalde, H. et al. IPCC Guidelines for National Greenhouse Gas Inventories. Volume 4: Agriculture,

662   Forestry and Other Land Use. Chapter 4: Forest Land. Forestry **4,** 1–29 (2006).

663   49.   Talbot, J. et al. Methods to estimate aboveground wood productivity from long-term forest inventory

664   plots. For. Ecol. Manage. **320,** 30–38 (2014).

665   50.   Clark, D. a et al. Measuring net primary production in forest concepts and field methods. Ecol. Appl.
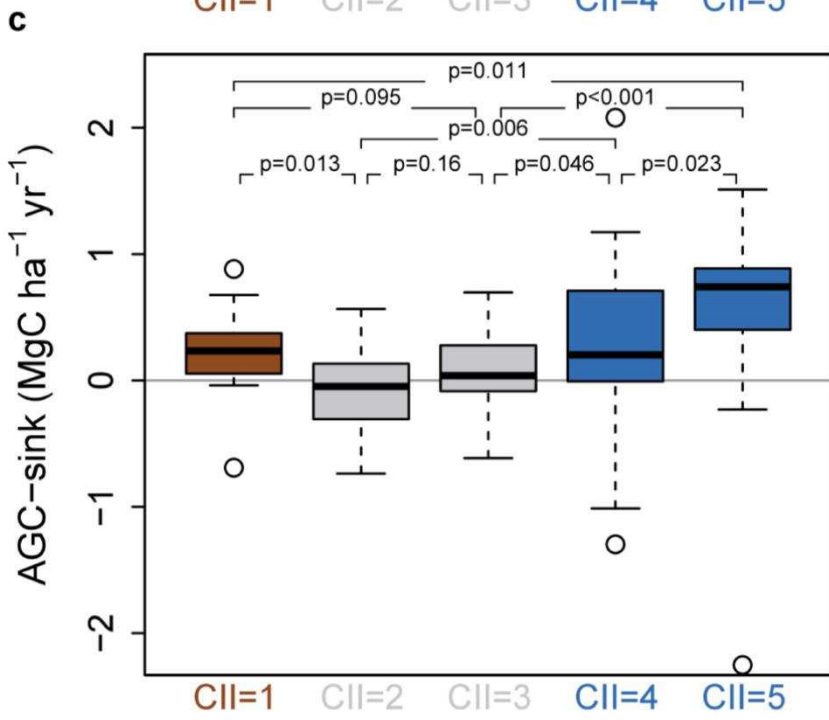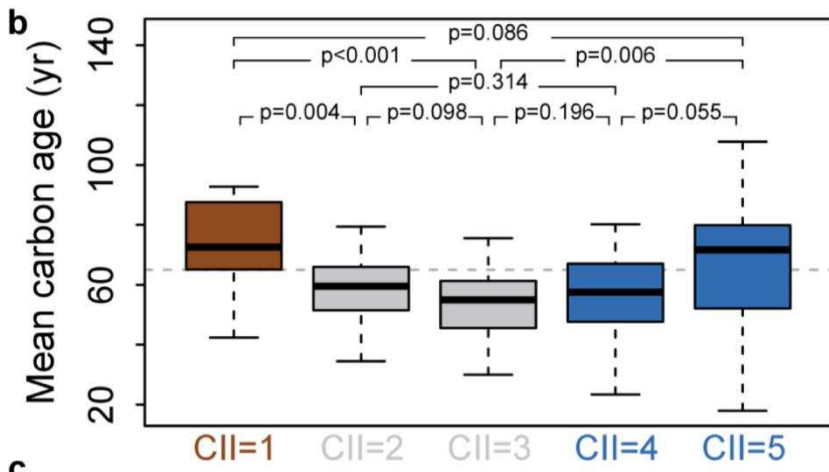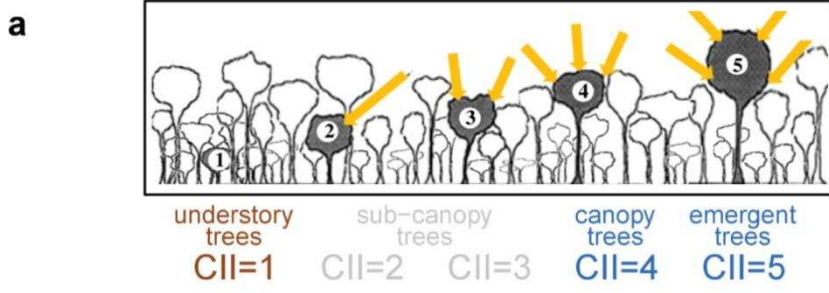
666   **11,** 356–370 (2001).

667

668

669

670

26